CO$_2$ Sequestration and Recycle by Photosynthesis

Final Report

September 24, 2001 – Septemeber 23, 2005

Steven S. C. Chuang

February 28, 2006

Department of Chemical Engineering, The University of Akron

200 East Buchtel Commons

Akron, OH, 44325-3906

Phone number: 330-972-6993; Fax number: 330-972-5856

E-mail: schuang@uakron.edu

Disclaimer

This report was prepared as an account of work sponsored by an agency of the United States Government. Neither the United States Government nor any agency thereof, nor any of their employees, makes any warranty express or implied, or assumes any legal liability or responsibility for the accuracy, completeness, or usefulness of any information, apparatus, product, or process disclosed, or represents that its use would not infringe privately owned rights. Reference herein to any specific commercial product, process, or service by trade name, trademark, manufacturer, or otherwise does not necessarily constitute or imply its endorsement, recommendation, or favoring by the United States Government or any agency thereof. The views and opinions of authors expressed herein do not necessarily state or reflect those of the United States Government or any agency thereof.

ABSTRACT

Hydrocarbon synthesis from photocatalytic reactions of CO_2 and H_2O over various catalysts has been studied by UV-visible light. The quantum efficiencies suggest that Pd/TiO_2 sol gel exhibits the highest activity for hydrocarbon synthesis from photocatalytic reactions. The in situ IR was able to monitor the adsorbed hydrocarbon species. The UV-visible, IR spectroscopy and XRD techniques were used to characterize the catalysts to obtain the information of properties of the process and catalyst before/after reaction. The UV-visible spectroscopy provides the information about the surface band gap energy of each catalyst. *In situ* UV-visible studies reveals that TiO_2-supported catalysts require the higher energy (i.e. shorter wavelength) to pass through the water-thin film deposited on the surface to activate the photocatalytic reaction. XRD data show there is changes in the crystal structure of TiO_2 sol gel from photon energy during photo reaction. Studies on photocatalytic oxidation of methylene blue show that the photocatalytic oxidation rate is significantly higher than the photocatalytic reduction rate on TiO_2 based catalysts. The information from this study can lead to a better understanding of the nature of the catalysts and photoreaction processes, which might provide the information to develop better catalysts and reaction process for the hydrocarbon synthesis from photocatalytic reactions of CO_2 and H_2O.

TABLE OF CONTENTS

LIST(S) OF GRAPHICAL MATERIALS

INTRODUCTION

Photocatalysis is a reaction process which involves the combined use of photon energy and catalytic surface sites to convert reactants to products. The reaction involves a number of key steps: (i) electronic excitation of semiconductor materials to produce electron/hole pairs, (ii) migration of electrons to the catalyst surface to reduce the reactant, and (iii) migration of holes to the catalyst surface to oxidize the reactant (1-4). The unique feature of photocatalysis is its ability to bypass conventional thermodynamic limitations, allowing significant conversion of reactants with low standard Gibbs free energy of formation, G^0_i, to products with high G^0_i. One of the most important photocatalytic conversions is the reaction of CO_2 with H_2O to produce methane and methanol (5-7). This reaction may be the key to developing a sustainable energy source because of depletion of fossil fuel reserves and continuous rise of CO_2 concentration in the atmosphere. The most promising catalysts are those that can be activated by visible light because approximately 90% of the energy emitted from the sun is in the visible region (8). Unfortunately, there has been little progress to-date on finding high activity, high selectivity catalysts which can catalyze this reaction under visible light.

The objective of this study is to determine the activity of the photocatalytic reaction of CO_2 and H_2O over Pd, Cu, and Rh based catalysts and the relation between the catalyst activity and the surface band gap. Group VIII metals exhibit activities for hydrocarbon synthesis during photocatalytic reactions. Loading noble metals such as Pd, Rh, Pt, Ag and Au on TiO_2 is reportedly to enable photocatalytic reactions by providing electron trapping sites on the catalyst surface (9-14). Cu has been used as an electron acceptor in TiO_2 aqueous suspensions because Cu has a work function quite similar to TiO_2 conduction band and standard reduction potential of oxygen molecule (15). Photocatalytic reactions in a slurry phase reactor are studied to determine

the reaction activity and selectivity for the different catalysts. An in situ infrared (IR) spectroscopy technique is used to determine adsorbate reactivities during the photocatalytic reaction. X-ray diffraction (XRD) and UV-visible spectroscopy methods are used to characterize the nature of the catalysts before and after reaction.

EXECUTIVE SUMMARY

Results of this study show that the Pd/TiO_2 solgel catalyst gave the highest activity for the photosynthesis of methane and methanol form CO_2/H_2O. However, the activity for this synthesis reaction is about 3 or 4 orders of magnitude lower than those of conventional catalysis. Comparison of photocatalytic oxidation and reduction shows that the photocatalytic oxidation rate is at least two orders of magnitude higher than the photocatalytic reduction on TiO_2-based catalysts. Development of a novel approach for the selective inhibition of the oxidation process is needed to accelerate the overall rate of the photosynthesis.

EXPERIMENTAL

Reduction

Catalyst preparation

0.5 wt% Cu/TiO_2, 0.5 wt% Rh/TiO_2, and 0.5 wt% $Cu/SrTiO_3$ catalysts were prepared by the incipient-wetness impregnation method. The 0.5 wt% Cu/TiO_2 was prepared by impregnating $CuCl_2$ (Sigma) in aqueous solution onto P25 TiO_2 (surface area: 50 m^2/g; Degussa), whereas the 0.5 wt% Rh/TiO_2 used $RhCl_2$ (sigma) with the same titania. The 0.5 wt% $Cu/SrTiO_3$ was prepared by impregnating $CuCl_2$ in aqueous solution onto $SrTiO_3$ (Alfa Aesar). Pd/SiC and Cu/SiC were prepared by incipient wetness impregnation of SiC (Alfa Aesar) with

6

aqueous solutions of $PdCl_2$ (Fisher Scientific) and $CuCl_2$ (Sigma), respectively. The ratio of the volume of salt solution to the weight of support is 1 cm^3:1 g. The impregnated samples were dried in air at 298 K for 24 h and calcined in 30 cm^3/min air flow at 773 K for 10 h.

The 2 wt% Pd/TiO_2 sol gel samples are prepared by adding 0.02 moles of $Ti(OC_4H_9)_4$ (Alfa Aesar) to a solution of 0.08 moles of n-butanol and 0.08 moles of acetic acid. This is followed by 8 h of stirring at 278 K under N_2 pressure, upon which $PdCl_2$ is added. The catalyst was then dried in air at 298 K for 24 h and calcined in 30 cm^3/min air flow at 773 K for 10 h.

Photocatalytic reaction in slurry-phase reactor

An Oriel 350 W Hg lamp (Model #6286) with associated power supply and housing was used as the source of the UV/visible light. Mercury lamps have a spectrum with many strong lines from 240 to 600 nm, followed by a declining continuum to 2.6 μm.

The photocatalytic activity of the CO_2/H_2O reaction for the production of hydrocarbons and oxygenates was studied on a number of catalysts using a modified 25-ml glass Erlenmeyer flask as a slurry reactor. The following catalysts have been tested in the slurry reactor under visible and UV-visible light irradiation at 225 mW/cm^2 intensity at 298 K and 0.1 MPa: TiO_2, Cu/TiO_2, Rh/TiO_2, SiC, Pd/SiC, Cu/SiC, $Cu/SrTiO_3$, and Pd/TiO_2 sol gel. For the slurry reactions, 500 mg of the catalyst and 10-ml deionized H_2O were charged in the reactor, along with a magnetic bar for mixing. The reactor was then flushed with 20 ml/min CO_2 flow for a period of 30 min and kept in batch mode for a period of 72 h. The gas samples were collected with respect to time and analyzed via gas chromatography (GC). Liquid samples were collected at the end of experiment and analyzed by GC and nuclear magnetic resonance (NMR) spectroscopy.

In situ IR studies of photocatalytic reaction

For in situ IR studies, a glass infrared reactor was used that consists of a T-shaped glass tube with a removable stainless steel flange at each end. The horizontal ends of the reactor are sealed by Viton O-rings with infrared-transparent (thallium bromoiodide) windows that allow the IR beam to pass through the reactor with a catalyst disk situated in the beam. A UV-visible transparent (CaF_2) window seals the top flange with a Viton O-ring, allowing exposure of the catalyst to radiation to initiate the reaction. The catalyst powders (25 mg) are pressed in the form of thin disks and placed in the reactor at a 45° angle on a stainless steel catalyst holder. This allows UV-visible light to excite the photocatalyst and simultaneous measurement of the variation of adsorbates and gaseous products with FTIR.

In order to increase the product formation to be detected via the IR, 100 mg of the catalyst was placed at the bottom of the reactor. Prior to placing the disk into the reactor, fours drops of water were added onto the catalyst disk and to the catalyst at the bottom of the reactor. The reactor was then flushed with 20 ml/min CO_2 flow for a period of 30 min and kept in batch mode. Thus, all background spectra are taken relative to the water-saturated disk. All in situ experiments were performed under UV-visible light at an intensity of 225 mW/cm^2.

Other Characterization Methods

Hewlett Packard (HP) 5890A and SRI 8601 gas chromatographs were used for quantification of gas and liquid samples. The HP 5890A GC used a 12' 80/100 Porapak Q column coupled with a flame ionization detector was used to determine the hydrocarbon products in both gas and liquid phase samples. T

he SRI 8601 GC with a capillary carboxen 1010 column and a thermal conductivity detector were utilized to determine the amount of O_2 produced. The GC is connected to an integrator for automatic determination of peak areas which, with use of calibration factors, can be converted to concentrations.

The catalysts were characterized by XRD with a Phillips APD3700 X-ray diffractometer equipped with a Cu K_α radiation source (wavelength 1.5406 A). Data are collected from 2° to 60° (2θ) with a step size of 0.02° and a time step 1.0 s to determine the crystallinity of the catalysts.

A Hitachi UV-visible spectrophotometer coupled with Harrick's Praying Mantis diffuse reflectance UV-visible cell was used to determine the absorption range of the catalysts. The catalyst powders were fully filled in the sample dish with a smooth surface on the top layer in order to obtain quality spectra. Absorption by the catalysts was measured from 190 - 800 nm with a scan speed of 60 nm/min. In situ UV-visible spectroscopy analysis in CO_2 and H_2O environments is also performed. The catalysts were crushed into fine powder and fully filled in the sample dish in the UV-visible cell. A dome with three CaF_2 windows is used to cover the reactor chamber. The CaF_2 window allows the UV-visible light to pass through the catalyst and reflect back to the detector. The mixture of CO_2 and H_2O vapor was brought into the reactor by flowing 20 cm^3/min CO_2 through a saturator. The UV-visible spectra were collected with the wavelength scan method to scan the absorbance of the sample from 800-190 nm with a scan speed of 60 nm/min.

<u>Oxidation</u>

TiO$_2$ was supplied by Degussa (P-25, surface area ~50 m^2/g; mean diameter ca. 30 nm; 80% anatase and 20% rutile); Methylene Blue (C$_{16}$H$_{18}$ClN$_3$S•3H$_2$O) from Alfa Aesar. Both compounds were used without further treatment.

Catalyst Preparation and Characterization

0.5 wt % Pt/TiO$_2$ was prepared by photo-reduction of K$_2$PtCl$_6$ onto TiO$_2$ in a solution containing ethanol which serves as a sacrificial electron donor. The specific procedure involves (i) bubbling N$_2$ through a 0.1 M ethanol solution containing K$_2$PtCl$_6$ and TiO$_2$ particles to remove O$_2$, (ii) illuminating the solution with a 350 W mercury UV lamp (Oriel 6286) for 24 hours while suspending TiO$_2$ particle in the solution by magnetic bar stirring, (iii) removal of Pt/TiO$_2$ from the solution by centrifuging, (iv) washing the particle with deionized water to remove Cl and K ion, (v) and drying under vacuum oven at 100 $^\circ$C. TiO$_2$ and 0.5 wt% Pt/TiO$_2$ were characterized by X-ray diffraction (Phillips APD3700 X-ray diffractometer equipped with a Cu K$_\alpha$ radiation source giving a wavelength of 1.5406 A) and UV-Vis spectroscopy UV-Visible spectrophotometer (HITACHI U-3010) equipped with a Praying Mantis diffuse reflectance accessory.

Photocatalytic Degradation of Methylene Blue in an Aqueous Solution

Photocatalytic degradation of Methylene Blue was studied with on two different modes. The first involves a square quartz reactor containing a 50 ml aqueous solution suspending with 5 mg of the catalysts under magnetic stirring; the second involves immobilizing the TiO$_2$ by

coating it on one side of the reactor wall by a slurry deposition technique.   The concentration of

MB was determined by UV-Vis spectroscopy.

In situ Infrared Study

50 mg of the reactant/catalyst mixture was placed in a DRIFT (diffuse reflectance) cell and

then exposed to a light from Xe lamp with an intensity of 16.7 mW/cm^2.   DRIFT spectrum was

taken by closing the movable light collector and interrupting the photocatalytic reaction,

RESULTS AND DISCUSSION

<u>Reduction</u>

Methane and methanol formation from photocatalytic reactions over Pd and Cu based catalysts

Figure 1 shows the quantity of methane formed with respect to time over Pd/SiC and

Pd/TiO$_2$ sol gel catalysts. The initial methane formation rate can be calculated from the slope of

the curves for the first 24 h and the average rate can be calculated from the accumulated amount

of methane divided by the total reaction time. Table 1 reports the initial and average methane

formation rate as well as the average methanol formation rate for all the catalysts in this study:

SiC, TiO$_2$, 0.5 wt% Pd/SiC, 2 wt% Pd/TiO$_2$ sol gel, 0.5 wt% Cu/SiC, 0.5 wt% Cu/TiO$_2$, 0.5 wt%

Cu/SrTiO$_3$, and 0.5 wt% Rh/TiO$_2$. Cu- and Rh-based catalysts exhibit high activities for

methanol and methane formation while Pd-based catalysts were highly selective toward methane.

The initial methane formation rates for all the catalysts were high at the onset except for Pd/TiO$_2$

sol gel, then proceeding to level off after 48 h of reaction time. Pd/TiO$_2$ sol gel exhibits a low

initial methane formation rate, which then increases after 24 h. After 48 h, the methane

formation rate for Pd/TiO$_2$ sol gel remains constant, whereas all other catalysts level off

11

This interesting difference may be attributed to changes in the Pd active sites and the conversion of TiO_2 sol gel crystal structure from rutile to anatase during the reaction. The latter is evidenced by XRD data shown in section 3.3. These changes might enhance the hydrocarbon formation rate, which explains the observation of an increasing methane formation rate for Pd/TiO_2 sol gel after 24 h.

In terms of the Pd-loading, Pd/TiO_2 sol gel has four times more Pd-loading than Pd/SiC. However, the average methane formation rate for Pd/TiO_2 sol gel is five times higher than that of Pd/SiC, which indicates that Pd/TiO_2 sol gel has a higher activity for methane formation than Pd/SiC and Cu-based catalysts. The order of methane formation activity from this study is: Pd/TiO_2 sol gel > Rh/TiO_2 > Cu/TiO_2 > Pd/SiC > Cu/SiC > Cu/$SrTiO_3$ > TiO_2 > SiC. The order of methanol formation activity is as followed: Cu/$SrTiO_3$ > Cu/TiO_2 > Cu/SiC > Rh/TiO_2 > Pd/SiC > Pd/TiO_2 sol gel > TiO_2 and SiC. These results show that different metal sites affect the selectivity of hydrocarbon formation during photocatalytic reactions. The literature reports that TiO_2 deposited on high-surface area mesoporous materials such as MCM-41 and MCM-48 could enhance the activity of the catalysts because more active sites are available (16). Combine with our data, this suggests that one method to boost the activity of the catalysts used in this study would be to deposit them on high-surface area supports.

Quantum efficiency

In order to determine the most active catalysts for methane/methanol formation, a fair comparison must be established between the results of this study and those reported in the literature. Quantum efficiency is the ratio of the product yield to the amount of photons

absorbed on the catalyst surface as defined in equation 1. This parameter is widely used to compare the efficiency of catalysts for photocatalytic reactions.

$$\phi_Q \ (\%) \ = \ \frac{\text{moles of required electron } \ x \ \text{ moles of hydrocarbon yield}}{\text{moles of UV photon absorbed by catalyst}} \ x \ 100 \qquad (1)$$

Moles of required electrons is the number of electrons needed to convert CO_2 to hydrocarbons. For example, conversion of C^{4+} in CO_2 to C^{4-} in CH_4 requires 8 electrons and conversion of CO_2 to CH_3OH requires 6 electrons. The moles of photons absorbed by the catalyst can be determined by diffuse reflectance UV-visible spectra, which indicate the range of light that can be absorbed by the catalyst. The band gap energy can be calculated from the wavelength as shown in equation 2 (17).

$$Energy \ (eV) \ = \ \frac{1.24 * 10^3}{Wavelength \ (nm)} \qquad (2)$$

Figure 2 shows the UV-visible spectra of the catalysts and the lowest energy of light that the catalysts can absorb. The moles of photons available for photosynthesis can be calculated from the area under the plot of Hg arc lamp emitted intensity vs. wavelength. The area under the plot is considered from 260 nm (the Erlenmeyer flask cuts off the UV-visible light below 260 nm) up to the wavelength of the light absorbed by the catalyst as determined by UV-visible spectroscopy. Figure 3 shows the spectral irradiance of the Hg arc lamp.

The calculation procedure of the number of photons is as follows; (i) determine the value of photon irradiance (I) in units of $mW.m^{-2}.nm^{-1}$ at each wavelength for the range of light that the catalyst can absorb, (ii) multiply each photon irradiance by the catalyst surface area that the light shines on and also by the wavelength to obtain the power output, P_λ (mW), at each wavelength as shown in equation 3:

$$P_\lambda = I.A.\lambda \qquad (3)$$

(iii) multiply the power output by the lens multiplication factor (0.11 for the UV-fused silica lens in the Hg lamp housing), and add 60% of that number due to the rear reflector in the lamp housing to obtain the actual power output from the lamp, P^*_λ, (iv) use equation 4 to obtain the number of photons per second at a particular wavelength, Φp:

$$\Phi p = P^*_\lambda.10^{-3}.\lambda.5.03 \times 10^{15} \qquad (4)$$

(v) sum Φp over the entire range that the catalyst can absorb to obtain the total number of photons per second as shown in equation 5:

$$\Phi_P^{Total} = \sum_{\lambda \geq 260nm} \Phi_P \qquad (5)$$

(vi) multiply the total number of photons per second by the reaction time to obtain the total number of photons that reach the catalyst (17)

Table 2 reports the quantum efficiency based on methane and methanol formation of the catalysts in this study. Pd/TiO$_2$ sol gel exhibits the highest methane quantum efficiency of 15.9% and a total quantum efficiency of 16.0%, which is 50% higher than 2.0 wt% Cu-TiO$_2$ sol gel reported in the literature (Wu). Cu/SrTiO$_3$ shows the highest methanol quantum efficiency of 1.5%.

Catalyst characterization

Most of the photocatalysis literature reports dry catalyst absorbance from diffuse reflectance UV-visible spectroscopy. The photocatalytic reactions in this study were carried out in a slurry phase reactor, not under dry conditions. Therefore the range of the light that can be absorbed by the catalyst might be affected by the CO_2 and H_2O environment. In order to study whether this effect is important, in-situ UV-visible spectroscopy experiments were carried out in CO_2 and H_2O vapor presence from the saturator.

Figure 4 shows the UV-visible spectra of 0.5 wt% Rh/TiO_2 in air and in a CO_2/H_2O environment. We find the absorbance of the catalyst shifts to higher energy (shorter wavelength), as evidenced by peak shifts from 340 and 370 nm to 305 and 350 nm, respectively, in the presence of CO_2/H_2O. The same experiment carried out in the presence of CO_2 alone shows no absorbance shifts. All the TiO_2-based catalysts in this study show the same behavior, while none of the SiC-based catalysts show absorbance shifts in the CO_2/H_2O environment. We postulate that the water forms a thin film on the surface of the TiO_2-based catalysts that blocks the low energy light from reaching the catalyst. This effect, not found in SiC-based catalysts, might be due to the hydrophobicity of SiC, which prevents the formation of a water film on the surface of the catalyst. The information from this study is useful for the design of catalytic reactions for the TiO_2-based photo-reduction of water.

XRD analysis can provide detailed information on the crystalline structure of the catalysts. The literature reports that TiO_2 powder changes its crystal structure from anatase-amorphous to anatase-rutile when it is calcined at high temperature (19-20). The catalyst crystal structure might also be changed due to photon absorption or catalytic reactions. Figure 5 shows XRD data from the catalysts before and after photoreaction. Figure 5 (a) shows the XRD pattern of SiC at a 2θ value of 35.5° and PdO at 45.5° (21). Figures 5 (b) and (c) show the patterns of Rh/TiO_2 and Cu/TiO_2. The anatase TiO_2 peaks were observed at 25°, 38°, 48° and 55° while rutile TiO_2 peaks were observed at 27.5°. Rh_2O_4 is identified by the peak at 41.5° and 44.5° (22) and CuO at 44.5° (18). In Figure 5 (d), the peak of $SrTiO_3$ is observed at 32°. After the reaction, these XRD patterns do not change, which indicates the crystal structure of these catalysts does not change during photochemistry.

Figure 5 (e) shows the XRD pattern of Pd/TiO$_2$ sol gel. The anatase TiO$_2$ sol gel peaks were observed at 25°, 38°, 48° and 55° while rutile TiO$_2$ sol gel peaks are present at 34°. Pd^0 and PdO are identified by the peaks at 40.5° and 44°, respectively (21). After photoreaction, the rutile peak of TiO$_2$ sol gel at 34° decreases and the anatase peak at 25° increases. These changes in relative intensity in the diffraction patterns indicate the change of the TiO$_2$ sol gel crystal structure from rutile to anatase during the photocatalytic reaction. The literature reports that the TiO$_2$ anatase crystal structure exhibits higher photocatalytic activity than the rutile crystal structure (23). The change in TiO$_2$ crystal structure from rutile to anatase observed in our XRD data and the two different types of Pd sites might promote the activity of the reaction and explain why this sol gel catalyst exhibits the highest activity for methane production.

Pd/SiC, Cu/TiO$_2$, Cu/SrTiO$_3$ and Pd/TiO$_2$ sol gel were pressed into the thin disks and analyzed via the IR to obtain the characteristic spectra for each catalyst. Figure 6 shows these IR spectra. Pd/SiC shows absorbance by the Si=C stretching at 800 cm^{-1} (24). TiO$_2$ and TiO$_2$ sol gel exhibit Ti-O stretching bands at 700 cm^{-1} (not shown) and Ti-O stretching in TiO$_4$ at 800 cm^{-1} (25-26). These IR spectra not only provide information on the catalyst structures, but also serve as reference data during the alignment procedure for the in situ IR studies discussed in the next section, where we must ensure that the IR beam pass through the catalyst disc.

In situ IR studies of the photocatalytic reaction over Cu/TiO$_2$ and Rh/TiO$_2$

Figure 7 shows IR spectra from the photocatalytic reaction over 0.5 wt% Cu/TiO$_2$ at 303 K and 0.15 MPa. Adsorbed hydrocarbon C-H stretching bands at 2935 and 2800 cm^{-1} are observed at 120 min reaction time. The gas-phase methane C-H stretching at 3055 cm^{-1} also emerges at 120 min and increases in intensity with respect to time. The same experiment carried out over 0.5 wt% Rh/TiO$_2$ results in adsorbed hydrocarbon C-H stretching bands at 2942 and

3165 cm^{-1} at 60 min reaction time as shown in Figure 8. Another hydrocarbon adsorbate with a C-H stretching mode at 2780 cm^{-1} also emerges at 180 min and increases the intensity with respect to time. From this study, we could successfully monitor the hydrocarbon adsorbates and product formation from the in situ IR technique. However the other intermediates or adsorbed species which needed to elucidate the reaction mechanism can not be detected. This might due to the low activity of these two catalysts as mentioned earlier.

Oxidation

Characterization

Figure 9 shows the approach for taking the infrared spectra of the catalysts and MB on catalyst under reaction conditions. Figure 10 shows the XRD patterns of TiO_2, 0.5 wt% Pt/TiO_2, 1 wt% Pt/TiO_2, and 3 wt% Pt/TiO_2.   XRD results shows that TiO_2 contains both anatase and rutile, confirming the P-25 structure; increasing the Pt content leads to an increase in the intensity of the Pt (111) peak at 39.8^{o}. The absence of Pt peak in 0.5 wt% TiO_2 suggests the Pt particle size on 0.5 wt% Pt/TiO_2 is less than 3 nm.

Figure 11 shows the results of the diffuse reflectance UV-Vis spectra of the TiO_2, 0.5 wt% Pt/TiO_2, 1 wt% Pt/TiO_2, and 3 wt% Pt/TiO_2. TiO_2 gave the absorption edge at 450 nm. The addition of Pt shifted the absorption edge to the lower wavelength and decreased the absorption. The latter could be resulted from increases in reflection from Pt metal particles.

Aqueous Phase Kinetic Study

Figure 12 shows the kinetics of MB photocatalytic degradation in an aqueous solution with suspending TiO_2 and 0.5 wt% Pt/TiO_2 particles. The rate of disappearance of MB fit well into the first order kinetics as shown in Fig. 5. This could be due to the presence of the significant excess H_2O which reduces the kinetic rate law into the pseudo first order form. The

rate constant obtained from fitting, listed in Table 3, is in the same order of magnitude with those reported in literature. In general, the rate constant depends on the catalyst composition and concentration as well as the wavelength and intensity of the illuminating light. Results in Fig. 12 and Table 3 show increasing the catalyst concentration increased the rate constant. The addition of Pt had little effect on the MB degradation.

Figure 13 shows the kinetics of MB degradation in an aqueous solution on TiO_2 and 0.5 wt% Pt/TiO_2 coating on the reactor wall. The objective of this study is to determine the photocatalytic oxidation kinetics in the absence of screening effect of the catalyst particles. The initial MB concentration was 30 ppm in the aqueous solution. 1.2 mg catalyst was coated on a surface of 4.5 cm^2

In situ Infrared Study

Figure 14 shows the key characteristic IR bands of MB on CaF_2, TiO_2, and 0.5wt% Pt/TiO_2. Methylene blue exhibits the aromatic ring C=C/C=N at 1599 cm^{-1}, C=C at 1488 cm^{-1}, C-H at 1388 cm^{-1}, the aromatic amine C_{Ar}-N at 1332 cm^{-1}, and the C-H wagging at 1250 cm^{-1}. The bands in 1400 – 1600 cm^{-1} became obscure for methylene blue on both TiO_2 and 0.5 wt% Pt/TiO_2 due to the strong IR absorption background of the TiO_2 catalysts. The IR bands observed in Figure 14 are summarized in Table 4. Both TiO_2 and Pt/TiO_2 exhibited a number of OH groups. These bands were attenuated after impregnating MB onto the catalysts.

Figure 15 shows the DRIFT spectra of MB on TiO_2 during photocatalytic degradation. Exposure of MB on TiO_2 to the UV illumination led to: (i) decrease in IR intensity of all the above bands as well as C-H at 2931 cm^{-1} and C=C in the aromatic ring at 1488 cm^{-1}; (ii) increase in IR intensity of the bands of C=O at 1718 cm^{-1} and N-H at 1576 cm^{-1}. The IR results suggested that MB photocatalytic oxidation proceeded the intermediates containing carbonyl functional

group (C=O) and produced ammonium ion (NH^{4+}).   Figure 16 shows photocatalytic degradation of MB on 0.5 wt% Pt/TiO_2. To compare the difference in the rate of change in IR intensity for both TiO_2 and 0.5 wt% Pt/TiO_2, the IR intensity of the MB bands was plotted in Figure 17. The presence of Pt accelerated the rate of decreases in the C_{Ar}-N band at 1332 cm^{-1} and increased the rate of formation of the N-H band at 1576 cm^{-1}.

CONCLUSIONS

The high rate of photocatalytic oxidation of MB on TiO_2 is an indication that the occurrence of the electron and hole separation do take place at an appreciable rate. The low rate of photocatalytic reduction reaction process can not be attributed to the low efficiency of electron and hole separation.   The low rate of photocatalytic reduction process could be due to the lack of the sites to transfer of electron and hole to the desirable adsorbed species and the high rate of the photocatalytic oxidation which convert the hydrocarbon and oxygenate products back to CO_2 and H_2O. Selective inhibition of photocatalytic oxidation is needed to improve the overall rate of the photocatalytic reduction process.

REFERENCES

1. Fox, M. A., Dulay, M. T., *Chem. Rev.* 93, 341 (1993).

2. Mahdavi, F., Bruton, T. C., Li Y., *J. Orgo Chem.* 58,744 (1993).

3. Jia, J., Ohno, T., Masaka, Y.; Matsumura, M. *Chem. Lett.,* 963, (1999).

4. Ohtani, B., Kusakabe, S., Okada, K., Tsuru, S., Nishimoto, S., Amino, Y., Izawa, K., Nakato, Y., Matsumura, M., Nakaoka, Y., Nosaka, Y. J *Chem. Soc. Perkin Trans.* 2, 201 (2001).

5. Anpo, M, and Matsuoka, M. *Journal of Photochemistry and Photobilogy* C: *Photochemistry reviews* 3, 225-252 (2003).

6. Ikeue, K., Nozaki, S., Ogawa, M., and Anpo, M., *Catalysis Letters.* 80, 111-114 (2002).

7. Anpo, M., Yamashita, H., Ichihashi, Y., and Ehara, S. *Journal of Electroanalytical Chemistry.* 396, 21-26 (1995).

8. Sze, S. M. in "Physics of Semiconductor Devices", 2nd ed. Wiley, New York, 1985.

9. Gao, Y-M.; Lee, W.; Trehan, R.; Kershaw, R.; Dwinght, K.; Wold, A. *Mater. Res. Bull.* 26, 1247 (1991).

10. Lee, W.; Shen, H-S.; Dwinght, K.; Wold, A. *J. Solid State Chem.* 106,288 (1993).

11. Wang, C-M.; Heller, A.; Gerischer, H. *J. Am. Chem. Soc.* 114,5230 (1992).

12. Driessen, M. D.; Grassian, V. H. *J. Phys. Chem. B* 102, 1418 (1998).

13. Hisanaga, T.; Harada, K.; Tanaka, K. *J. Photochem. Photobiol. A: Chem.* 54,113 (1990).

14. Borgarello, E.;Pelizzetti, E. *Inorg. Chim. Acta* 91, 295 (1984).

15. Gerischer, H.; Seller, A. *J. Phys. Chem.* 95,5261 (1991).

16. Yamashita, H., Fukii, Y., Ichihashi, Y., Zhang, S. G., Ikeue, K., Park, D. R., Koyano, K., Tatsumi, T., Anpo, M., *Catalysis Today,* 45, 221 (1998).

17. The Book of Photon Tools: Oriel Insturment, pp. 1.2-1.4, 1.56-1.57.
'
18. Tseng, I. H., Chang, W., and Wu, J., *Appl. CataI. B: Environ.* 37,37-48 (2002).

19. Bessekhouad, Y., Robert, D., Weber, J. V. *J. of Photochemistry and Photobiology A:Chemistry, 15, 47-53 (2003).*

20. Tanaka, Y. and Suganuma, M. *J. of Sol-gel Sci. and Tech.* 22, 83-89 (2001).

21. Bi, Y. and Lu. G., *Applied Catal. B: Environ.* 41,279-286 (2003).

22. Niemantsverdriet, J. W. in "Spectroscopy in Catalysis", 2nd ed., Wiley, New York, 2000.

23. Linsebigler, A. L., Lu, G., and Yates, T. *Chem. Rev.* 95,735-758 (1995).

24. Hobert, H. *Vibrational spectroscopy* 19, 205-211 (1999).

25. Abdel-Shafi, N and Morsi, M. M. *J. of material sciences* 32, 5185-5189 (1997).

26. Wachs, I. E. *Catalysis Today* 27,437-455 (1996).

27. Zhang, T.; Oyama, T.; Aoshima, A.; Hidaka, H; Zhao, J.; Serpone, N., *Journal of Photochemistry and Photobiology A: Chemistry*, 140, 163 (2001).

28. Lachheb, H.; Puzenat, E.; Houas, A.; Ksibi, M.; Elaloui, E.; Guillard, C.; Herrmann, J., *Applied Catalysis B: Environmental*, 39, 75 (2002).

29. Zhang, T.; Oyama, T.; Horikoshi, S.; Hidaka, H.; Zhao, J.; Serpone, N., *Solar Energy Materials & Solar Cells*, 73, 287 (2002).

30. Lakshmi, S.; Renganathan, R.; Fujita, S., *Journal of Photochemistry and Photobiology A: Chemistry*, 88, 163 (1995).

31. Supsakulchai, A.; Ma, G.; Nagai, M.; Omi, S., *J. Microencapsulation*, 20, 19 (2003).

32. Inagaki, M.; Imai, T.; Yoshikawa, T.; Tryba, B., *Applied Catalysis B: Environmental*, 51, 247 (2004).

33 Li, X.; Li, F.; Yang, C.; Ge, W., *Journal of Photochemistry and Photobiology A: Chemistry*, 141, 209 (2001).

34. Li, F.; Li, X., *Chemosphere*, 48, 1103 (2002).

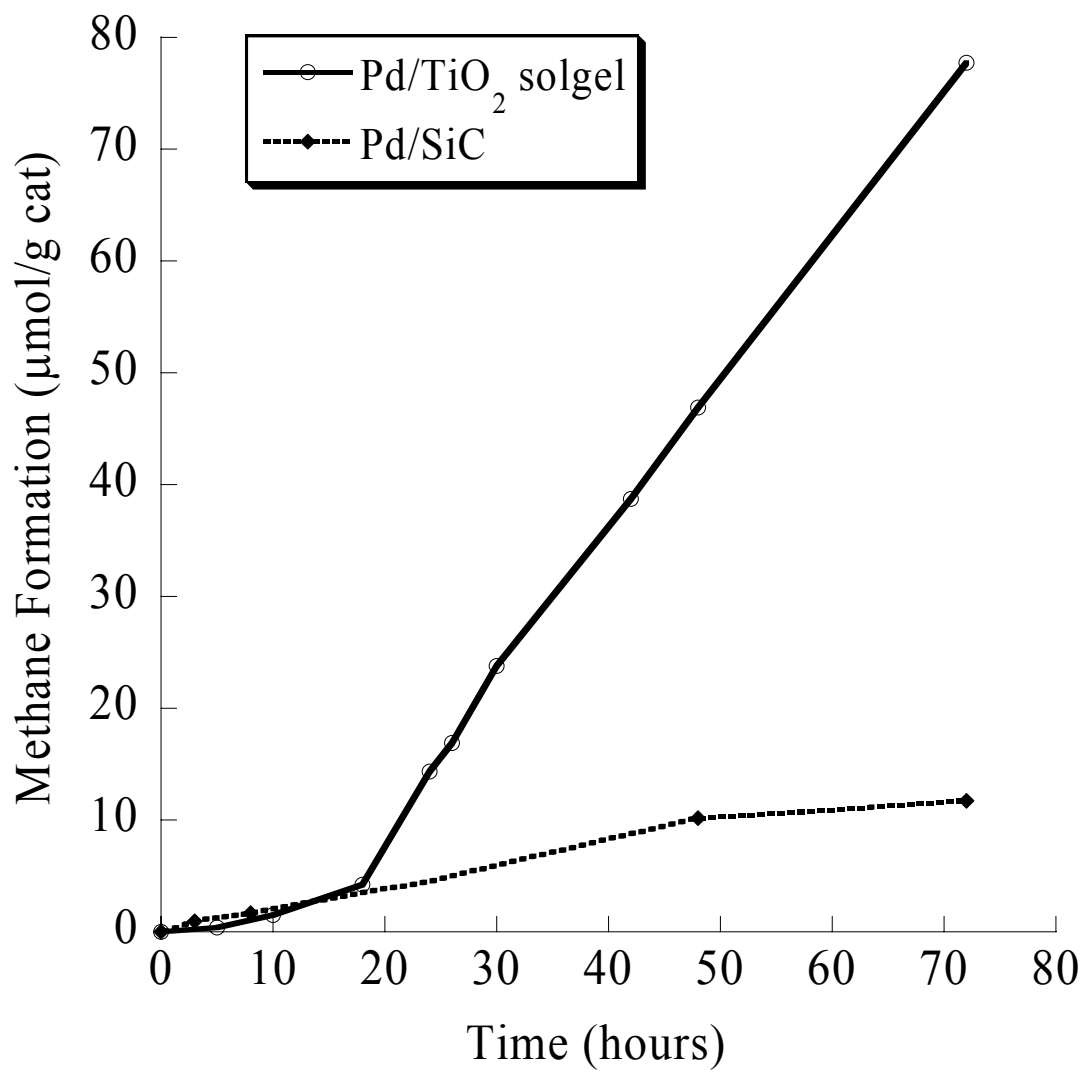35. Li, F.; Li, X., *Applied Catalysis A: General*, 228, 15 (2002).
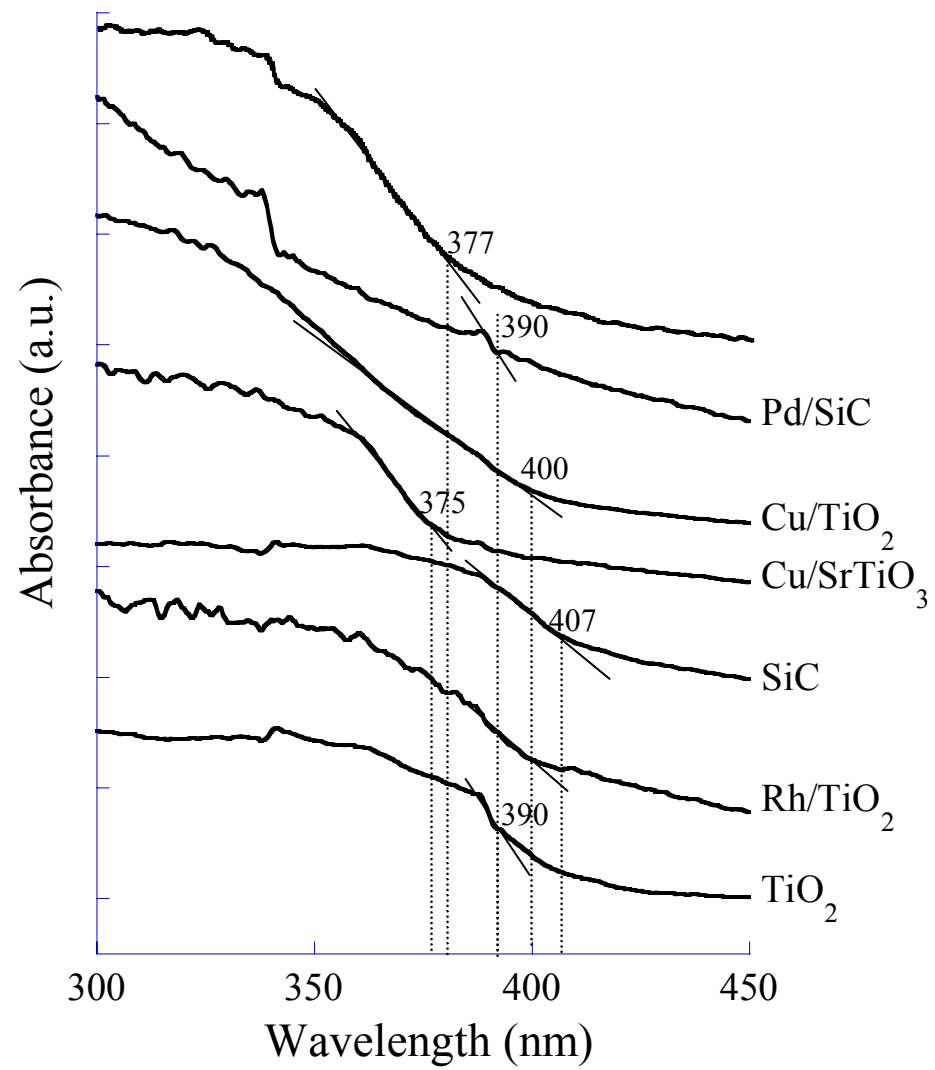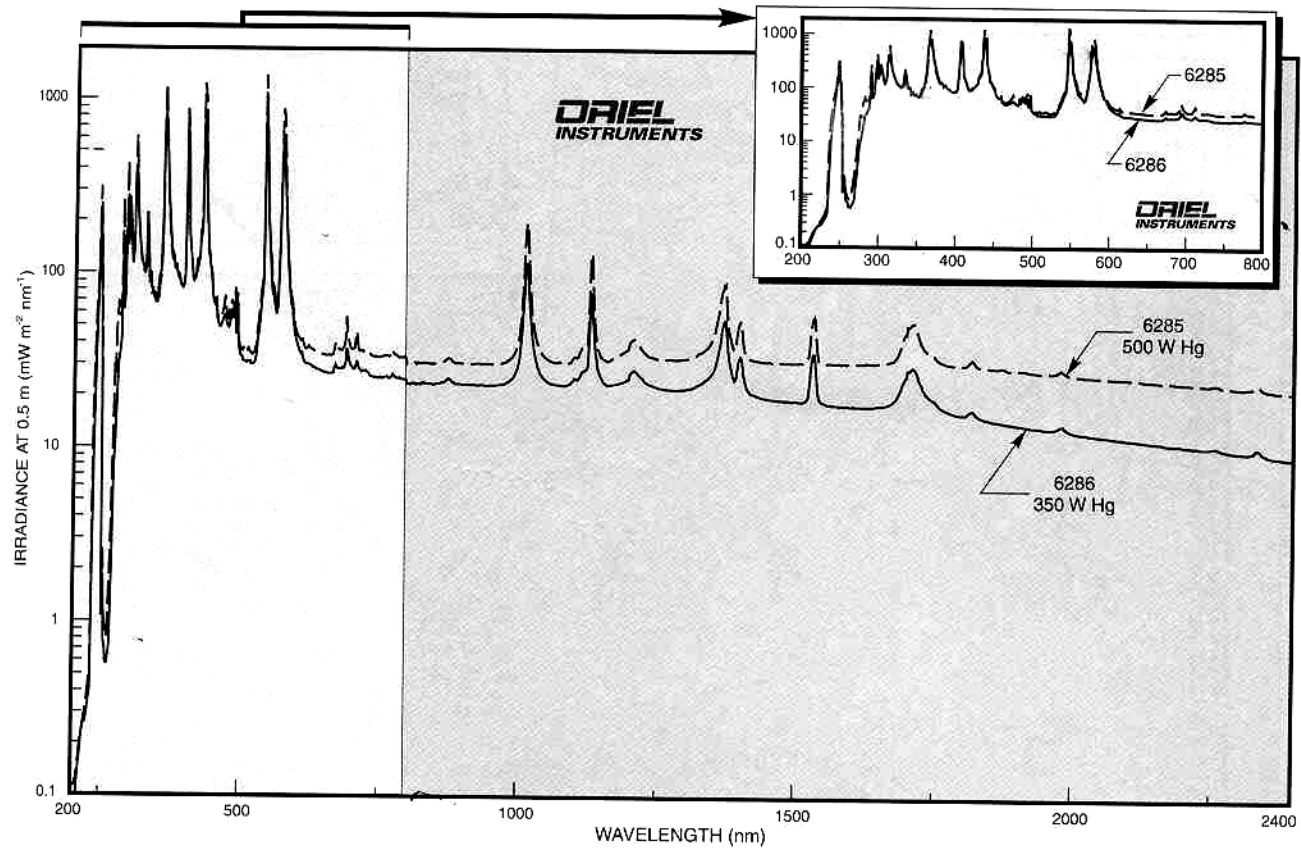
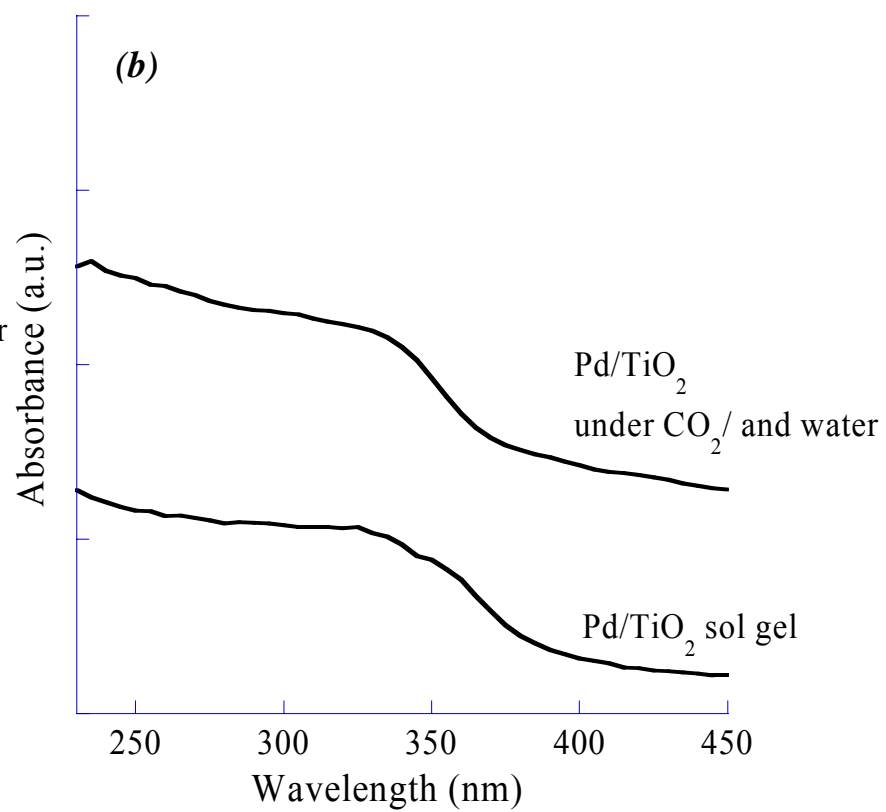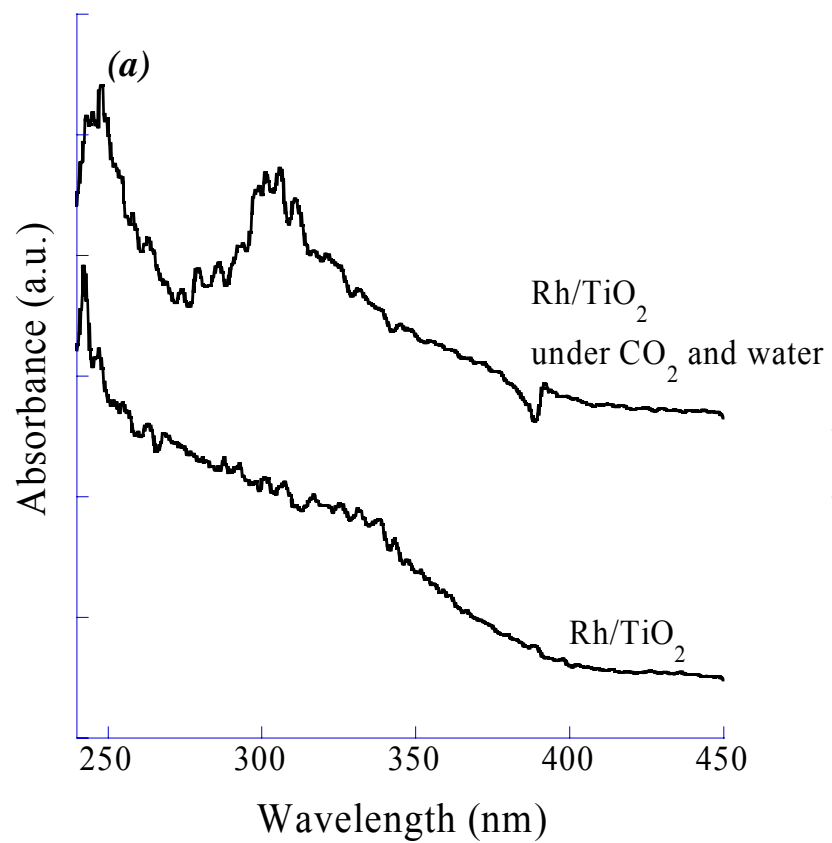36. Li, X.; Li, F., *Environ. Sci. Technol.*, 35, 2381 (2001).

20

Figure 1

Figure 2

Figure 3

Figure 4

Figure 5

Pd/TiO$_2$ sol gel

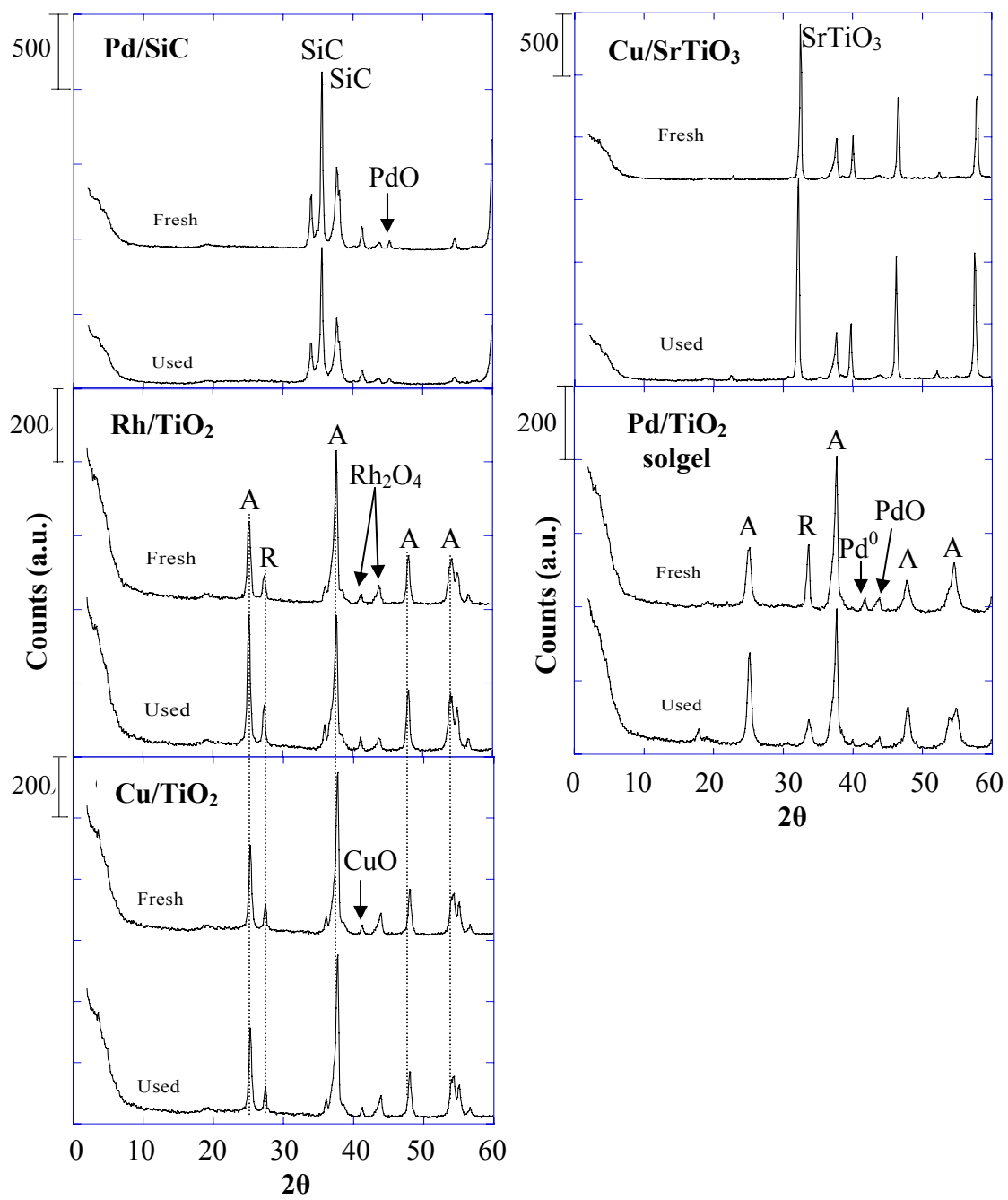Cu/SrTiO$_3$

Cu/TiO$_2$

Pd/SiC
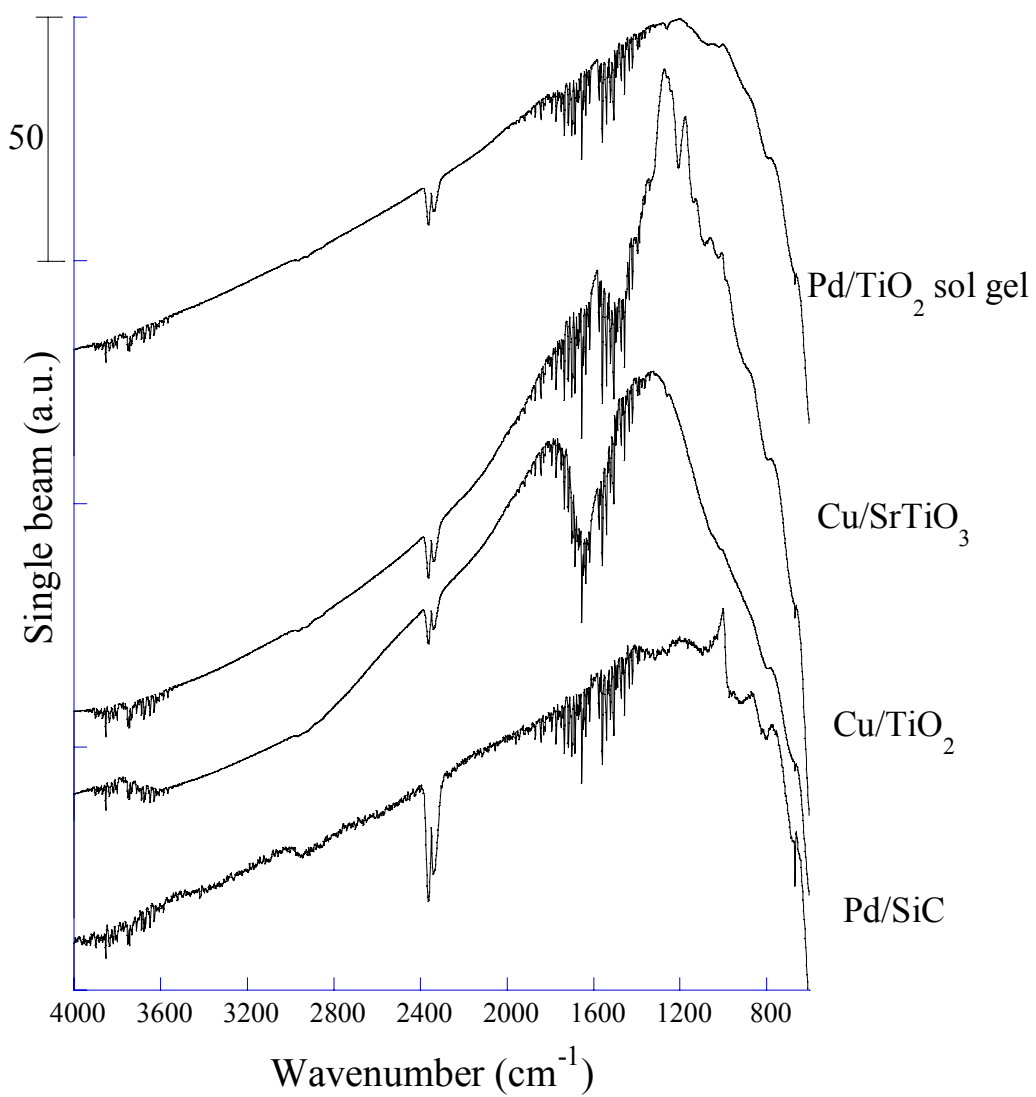
Single beam (a.u.)

50

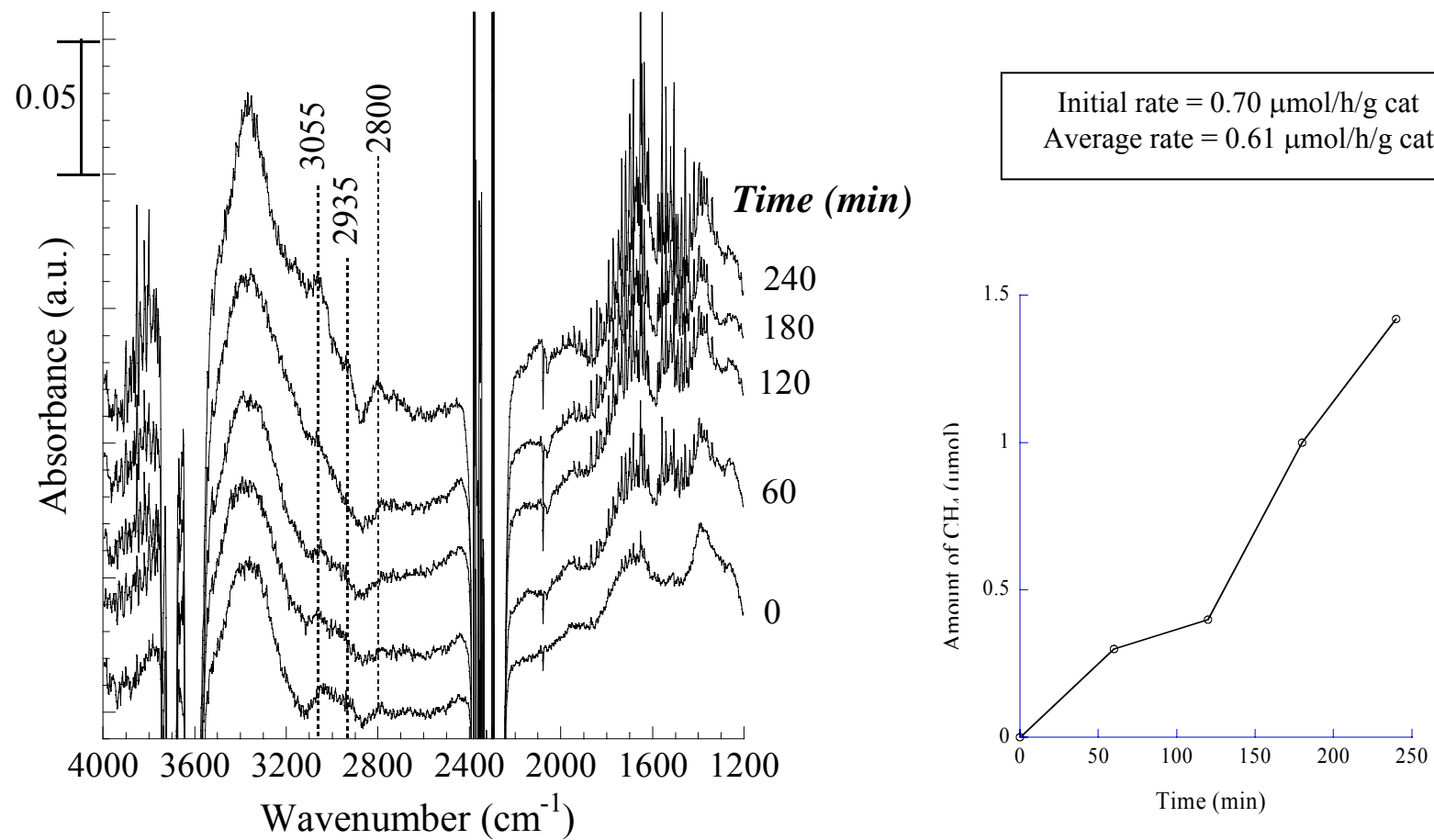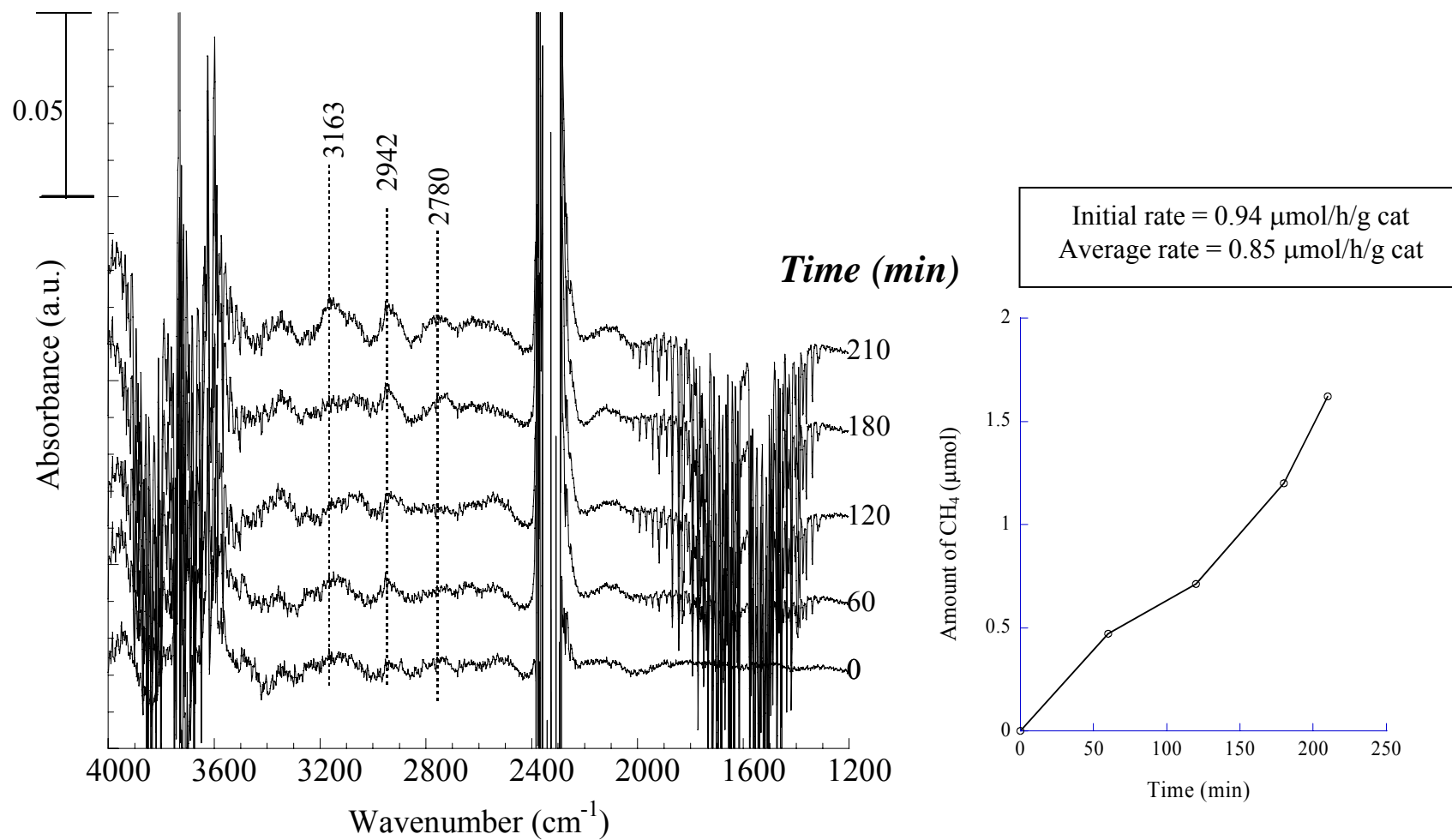Wavenumber (cm^{-1})

26

Figure 6

Figure 7

Figure 8

Table 1 Hydrocarbon formation rates from photocatalytic reactions over various catalysts.

Catalyst	Initial rate of CH_4 formation ($\mu mol/hr/gcat$)	Average rate of CH_4 formation ($\mu mol/hr/gcat$)	Average rate of CH_3OH formation ($\mu mol/hr/gcat$)	T (K)	Light Range / Intensity
SiC	0.05	0.05	0.000	303	$\lambda > 260$ nm/225 W
TiO_2 (P25)	0.10	0.10	0.000	303	$\lambda > 260$ nm/225 W
0.5 wt% Pd/SiC	0.33	0.25	0.007	303	$\lambda > 260$ nm/225 W
2.0 wt% Pd/TiO_2 sol gel	0.25	1.16	0.006	303	$\lambda > 260$ nm/225 W
0.5 wt% Cu/SiC	0.28	0.20	0.140	303	$\lambda > 260$ nm/225 W
0.5 wt% Cu/TiO_2	0.43	0.28	0.300	303	$\lambda > 260$ nm/225 W
0.5 wt% Cu/$SrTiO_3$	0.15	0.15	0.630	303	$\lambda > 260$ nm/225 W
0.5 wt% Rh/TiO_2	0.73	0.38	0.120	303	$\lambda > 260$ nm/225 W
Literature					
1.0 wt% Cu/TiO_2 [3]	N/A	0.00	0.006	323	$\lambda > 280$ nm / 75 W
TiO_2 (P25) [13]	N/A	0.25	0.000	328	$\lambda > 250$ nm / 75 W
Ti-MCM-41 [14]	N/A	2.00	0.750	328	$\lambda > 260$ nm / N/A
Ti-MCM-48	N/A	2.00	1.000	328	$\lambda > 260$ nm / N/A

Table 2 Quantum efficiency (Φ_Q) of the photocatalytic reaction over various catalysts.

Catalyst	CH$_4$ Quantum Efficiency	CH$_3$OH Quantum Efficiency	Quantum Efficiency (Φ_Q)	T (K)	Light Range / Intensity
SiC	0.55	0.0	0.55	303	$\lambda > 260$ nm/225 W
TiO$_2$ (P25)	1.13	0.0	1.13	303	$\lambda > 260$ nm/225 W
0.5 wt% Pd/SiC	3.96	0.015	3.98	303	$\lambda > 260$ nm/225 W
2.0 wt% Pd/TiO$_2$ sol gel	15.93	0.017	15.95	303	$\lambda > 260$ nm/225 W
0.5 wt% Cu/SiC	3.11	0.30	3.41	303	$\lambda > 260$ nm/225 W
0.5 wt% Cu/TiO$_2$	4.80	0.64	5.44	303	$\lambda > 260$ nm/225 W
0.5 wt% Cu/SrTiO$_3$	1.94	1.53	3.47	303	$\lambda > 260$ nm/225 W
0.5 wt% Rh/TiO$_2$	8.19	0.25	8.44	303	$\lambda > 260$ nm/225 W
Literature[18]					
TiO$_2$ (P25)	N/A	3.41	3.41	298	$\lambda = 254$ nm/8 W
2.0 wt% Cu/TiO$_2$ (P25)	N/A	5.35	5.35	298	$\lambda = 254$ nm/8 W
1.0 wt% Cu/TiO$_2$ sol gel	N/A	6.06	6.06	298	$\lambda = 254$ nm/8 W
2.0 wt% Cu/TiO$_2$ sol gel	N/A	10.02	10.02	298	$\lambda = 254$ nm/8 W

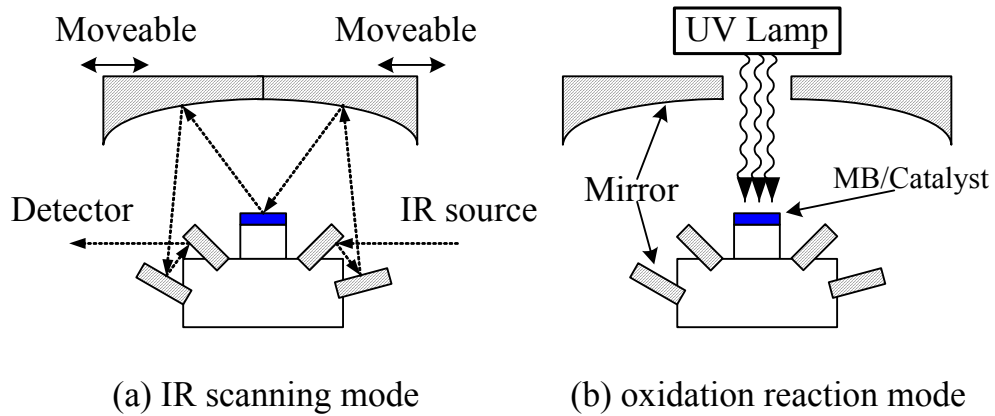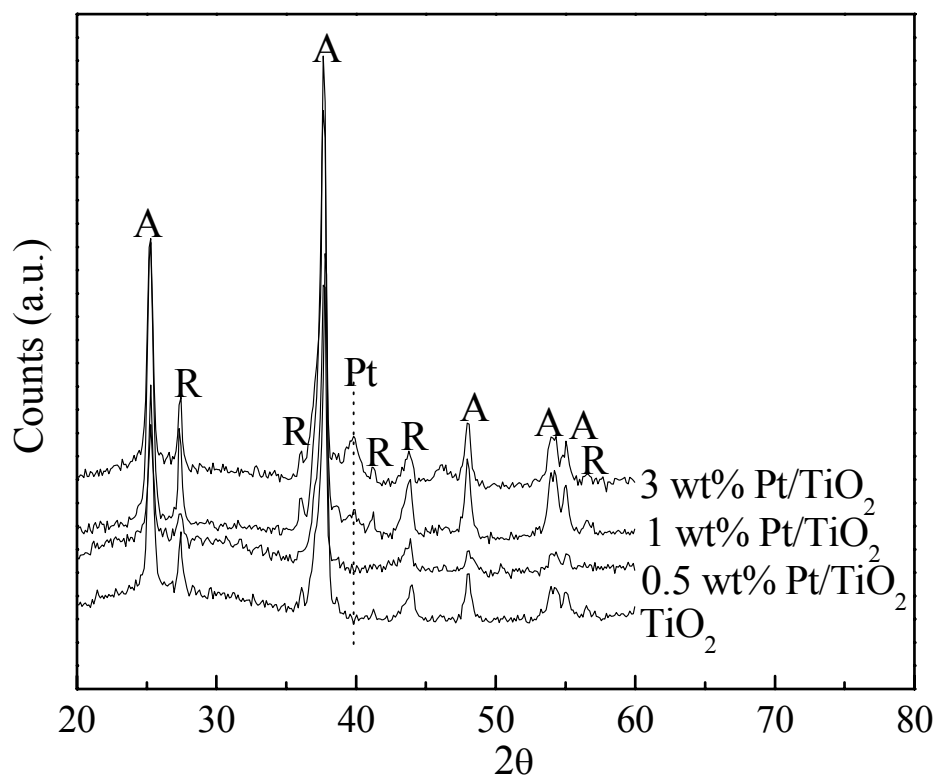(a) IR scanning mode   (b) oxidation reaction mode

Fig. 9. Schematic diagrams of MB photocatalytic oxidation on Diffuse
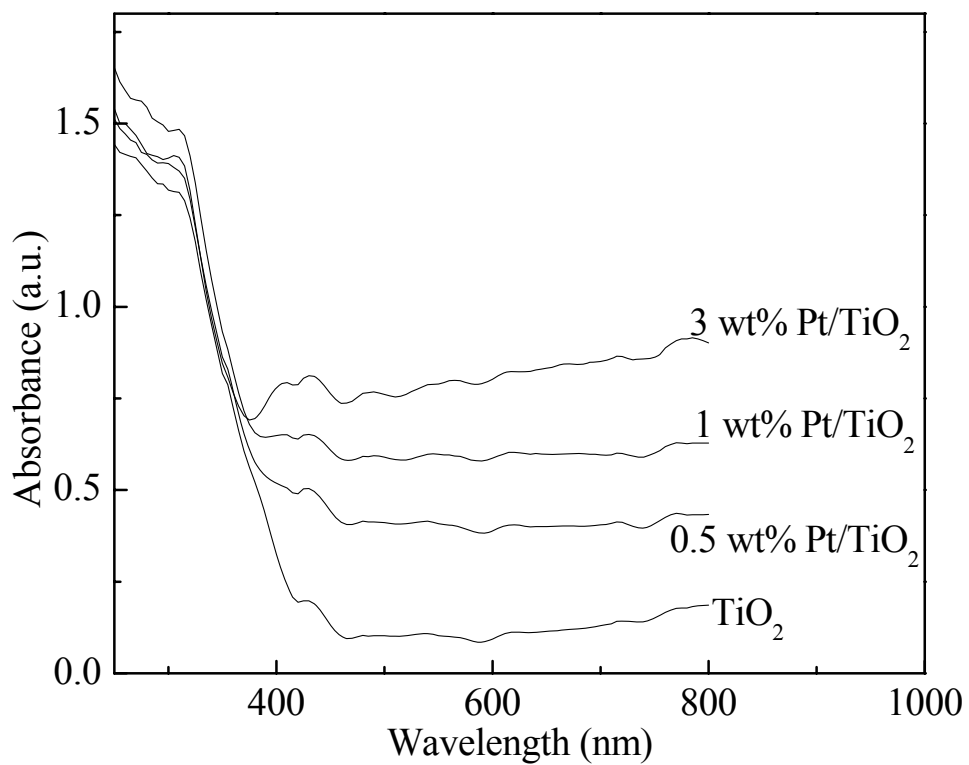Reflectance Infrared Fourier Transform Spectroscopy reactor.

Fig. 11. UV-vis diffuse reflectance spectra of pure TiO_2, 0.5 wt%
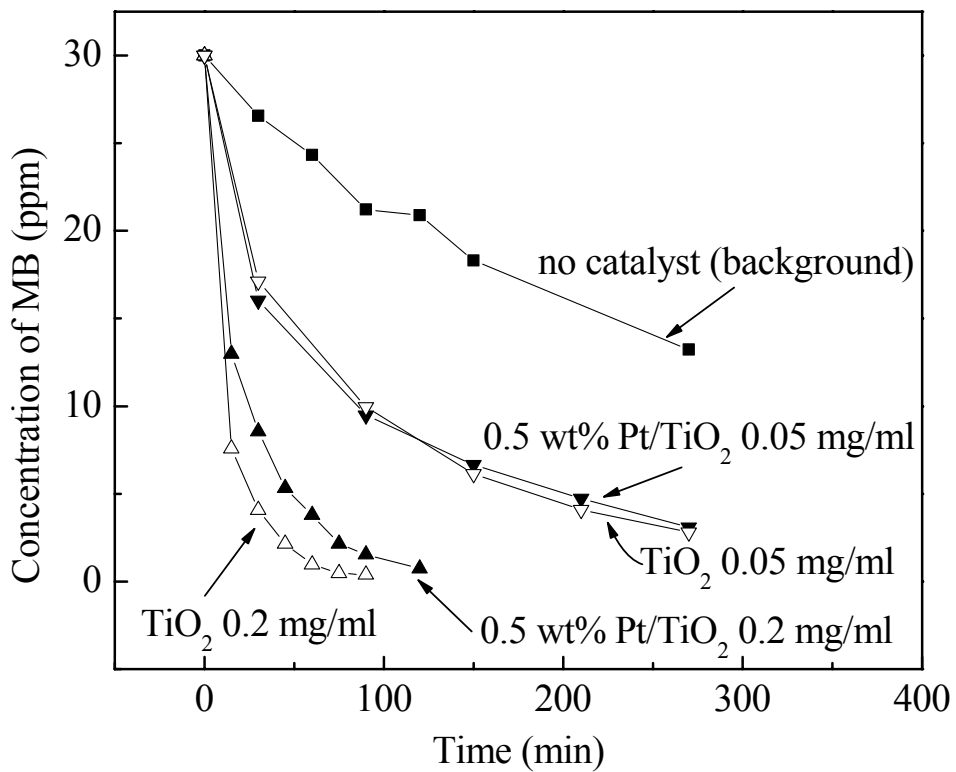Pt/TiO_2, 1 wt% Pt/TiO_2 and 3 wt% Pt/TiO_2.

Fig. 12. Concentrations of MB as a function of time in photocatalytic oxidations of MB in aqueous solution with non-catalyst, pure TiO_2, and 0.5 wt% Pt/TiO_2. Two catalyst concentrations, 0.05 mg/ml and 0.2 mg/ml were tested.
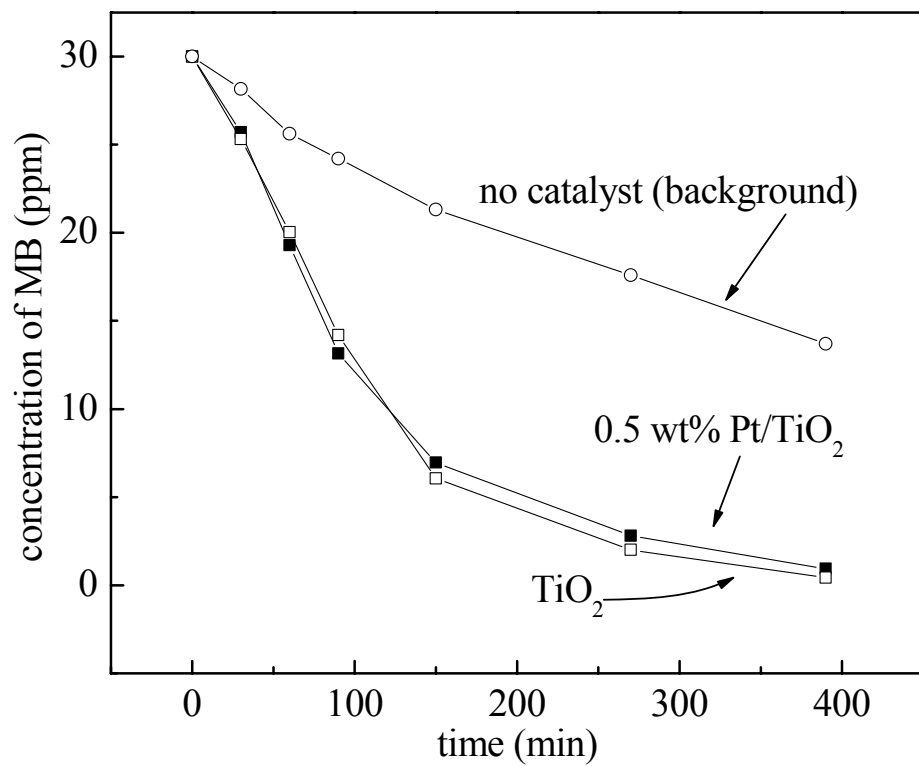
Fig. 13. Photocatalytic oxidation of MB in liquid-thin film system with non-catalyst, P25, and 0.5 wt% Pt/P25.
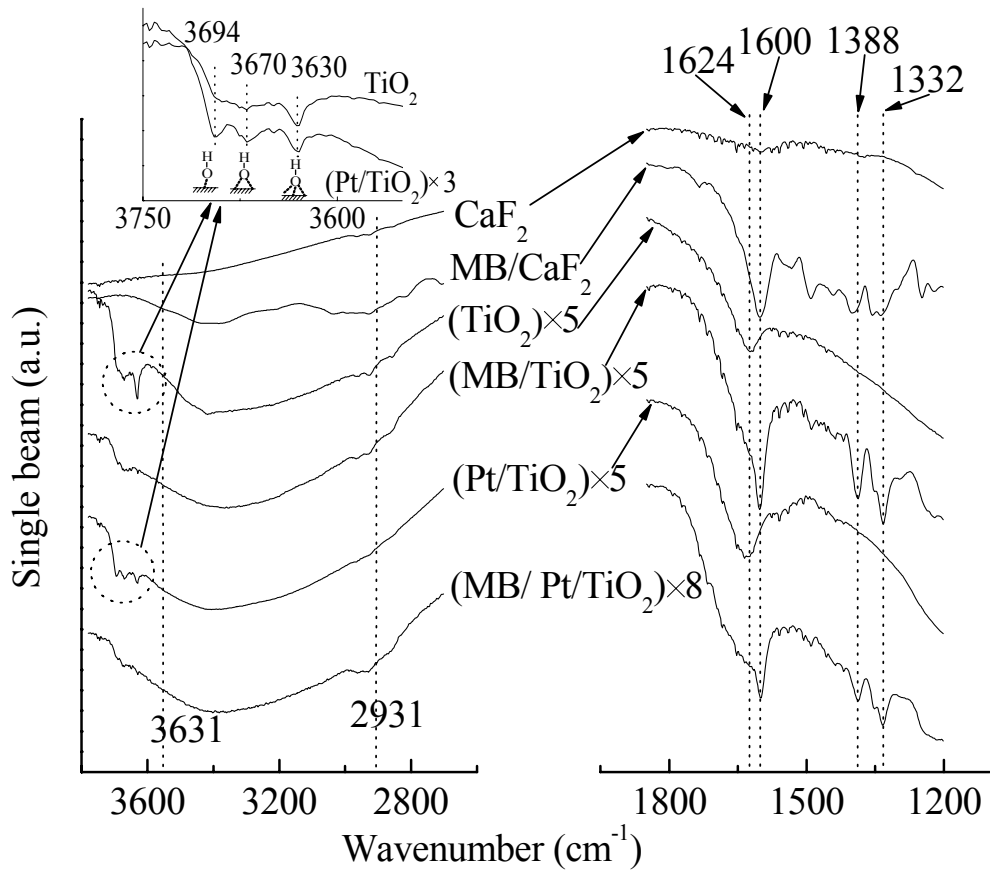
Fig.14. IR backgrounds of CaF$_2$ and MB/CaF$_2$, TiO$_2$ and MB/TiO$_2$, 0.5 wt% Pt/TiO$_2$ and MB/ 0.5 wt% Pt/TiO$_2$. The insert shows the different types of isolated hydroxyl group over TiO$_2$ and 0.5 wt% Pt/TiO$_2$ surfaces. indicates the spectrum is enlarged by a certain factor.
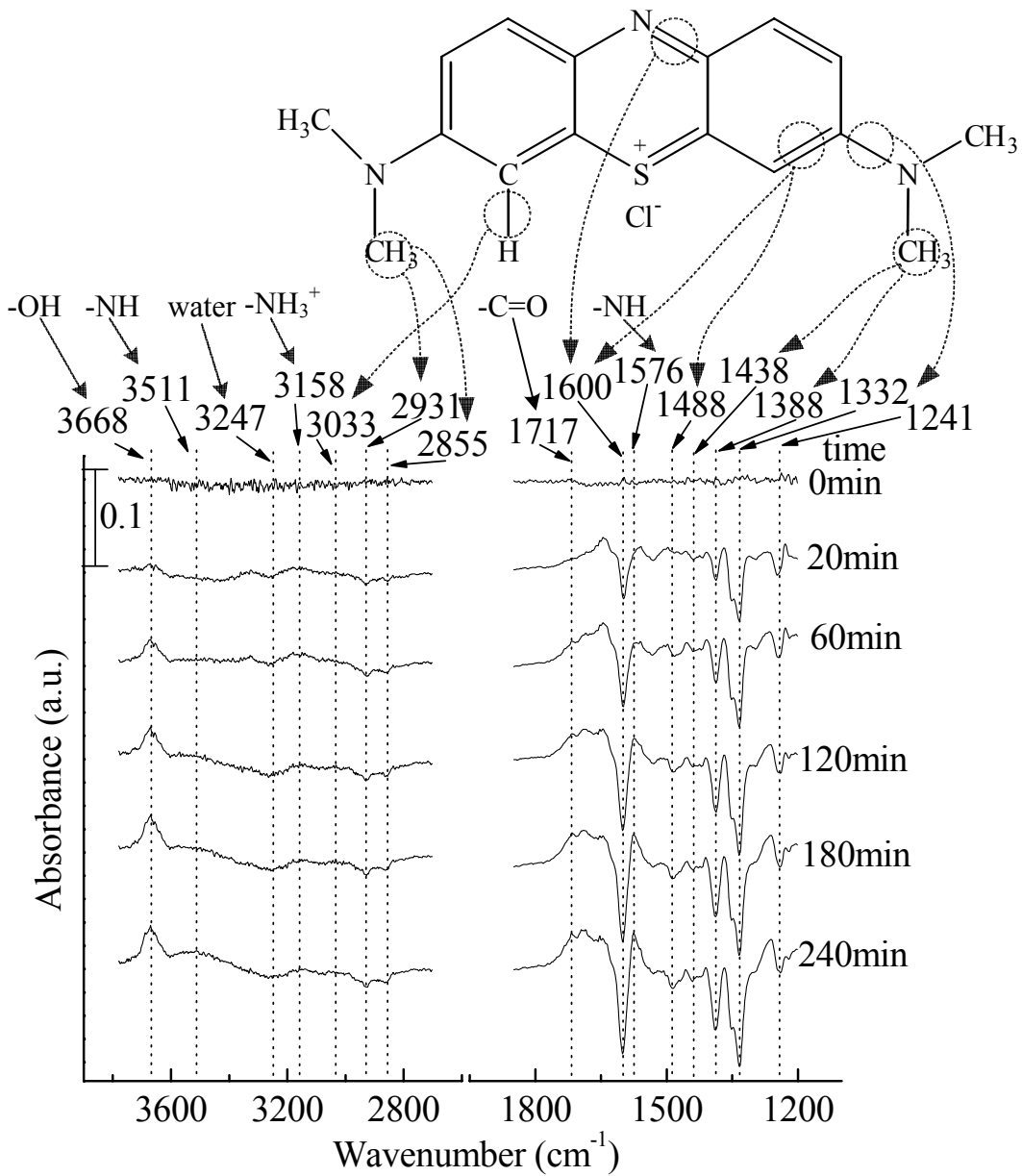
Fig. 15. In situ DRIFTS spectra and band assignments of MB photocatalytic oxidation over pure TiO$_2$ with 5 wt% MB at 1 atm and 25 ºC.
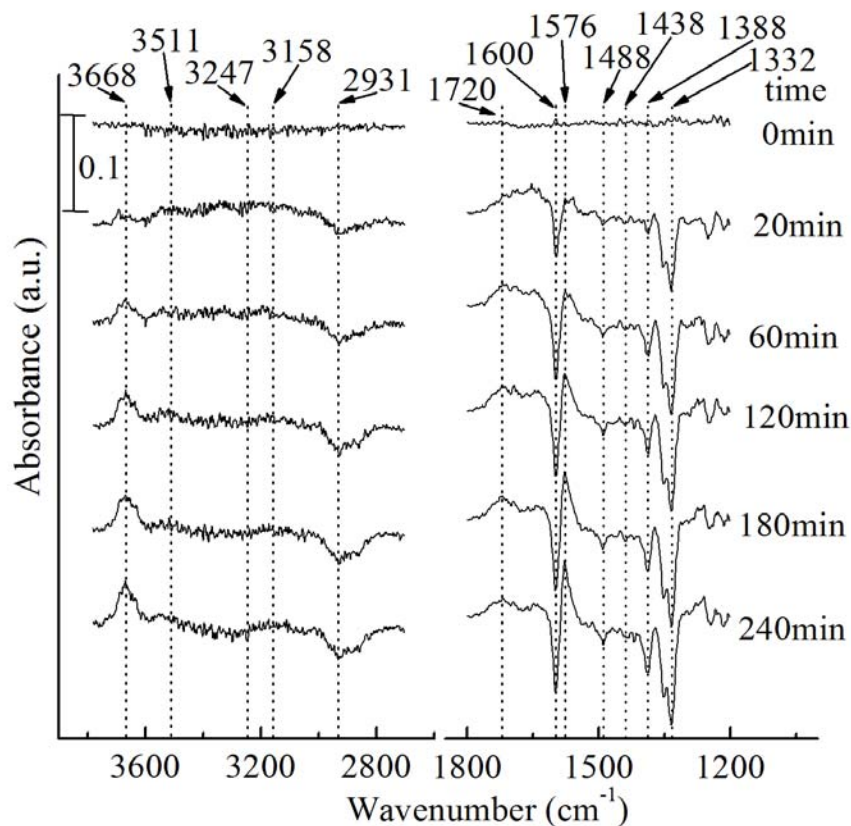
Fig. 16. In situ DRIFTS spectra of MB photocatalytic oxidation over 0.5 wt% Pt/TiO$_2$ with 5 wt% MB at 1 atm and 25 ºC.
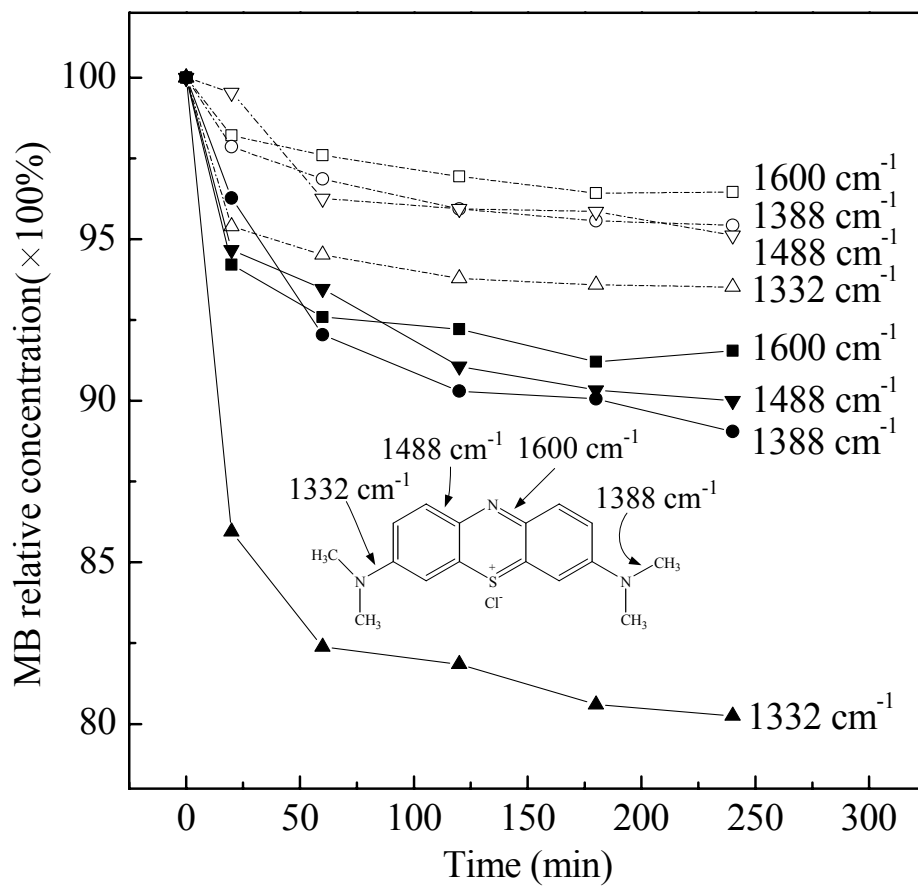
Fig. 17. Decrease rates of MB characteristic bands as a function of time in the MB photocatalytic oxidation over pure TiO$_2$ (dash line and empty symbol) and 0.5 wt% Pt/TiO$_2$ (black line and solid symbol) with 5 wt% MB at 1 atm and 25 ºC.

Table 3: literature review for MB photocatalytic oxidation in aqueous solution

catalyst	Reaction conditions: C_{MB0}, C_{cat}, I	Kinetics model and reaction constant, k	reference
P25 (30nm)	C_{MB0}=93.8 µmol/l C_{cat}=0.2 g/l I=16.7mW/cm^2	first-order kinetics k=0.048 min^{-1}	This report
P25 (30nm)	C_{MB0}=100 µmol/l C_{cat}=2 g/l I=4.7mW/cm^2	first-order kinetics k=0.032 min^{-1}	27
P25 (30nm)	C_0=84.2 µmol/l C_{cat}=0.5 g/l I= N/A	first-order kinetics k=0.053 min^{-1}	28
P25 (30nm)	C_0=25 µmol/l C_{cat}=2 g/l I: N/A	first-order kinetics k=0.078 min^{-1}	29
P25 (30nm)	C_0=6.6 µmol/l C_{cat}=0.67 g/l I: N/A	first-order kinetics k=0.0288 min^{-1}	30
TiO$_2$ (50 nm)	C_0=20 µmol/l C_{cat}=0.218 g/l I=N/A	first-order kinetics k=0.004 min^{-1}	31
TiO$_2$ (20 nm)	C_0=31.3 µmol/l C_{cat}=1 g/l I=N/A	first-order kinetics k=0.025 min^{-1}	32
TiO$_2$ (29.5 nm)	C_0=39.1 µmol/l C_{cat}=1.2 g/l I=N/A	first-order kinetics k=0.0188 min^{-1}	33
TiO$_2$ (20 nm)	C_0=46.9 µmol/l C_{cat}=1.2 g/l I=N/A	first-order kinetics k=0.0672 min^{-1}	34
0.75 wt% Pt/TiO$_2$ (40-80 nm)	C_0=46.9 µmol/l C_{cat}=1.2 g/l I=N/A	first-order kinetics k=0.1042 min^{-1}	34
TiO$_2$ (18.3 nm)	C_0=62.6 µmol/l C_{cat}=1.2 g/l I=N/A	first-order kinetics k=0.0955 min^{-1}	35
0.5 wt% Au/TiO$_2$ (11.8-14.2nm)	C_0=62.6 µmol/l C_{cat}=1.2 g/l I=N/A	first-order kinetics k=0.1752 min^{-1}	35
TiO$_2$ (18.3 nm)	C_0=37.5 µmol/l C_{cat}=1.2 g/l I=N/A	first-order kinetics k=0.0144 min^{-1}	36
0.5 wt% Au/TiO$_2$ (19.4 nm)	C_0=37.5 µmol/l C_{cat}=1.2 g/l I=N/A	first-order kinetics k=0.052 min^{-1}	36

C_{MB0}: initial concentration of MB in solution.
C_{cat}: concentration of catalyst in reaction solution.
I: light intensity.

Table 4: assignment of the FTIR bands observed in MB
photocatalytic oxidation over TiO_2 at 1 atm and 25 ºC.

Frequency (cm^{-1})	Vibration mode of functional group
3668	-OH
3511	-NH
3247	Absorbed water
3158	$-NH_3^+$
3033	Aromatic C-H
2931	$-CH_3$ asymmetric stretching
2855	$-CH_3$ symmetric stretching
1718	-C=O
1600	C=N/C=C
1576	-N-H
1488	C=C
1438	$-CH_3$ asymmetric deformation
1388	$-CH_3$ symmetric deformation
1333	Aromatic amines, C_{Ar}-N